Three-Dimensional Magnetohydrodynamic Analysis of a Magnetic Sail Using a Deployable Modular Structure

Three-Dimensional MHD Analysis of a Magnetic Sail Using a Deployable Modular Structure

Shoko Arita[1] and Yoshiki Yamagiwa[2]
Shizuoka University, Hamamatsu, Shizuoka, 432-8011, Japan

To obtain significant drag from a magnetic sail, it is necessary to generate a large magnetic moment. However, even with superconducting coils, a coil radius of several kilometers is required to obtain a significant drag force due to the magnetic moment generated by the coil alone. Therefore, several methods have been proposed to expand the magnetosphere generated by the coil, such as mini-magnetospheric plasma propulsion devices. This paper proposes a method to expand the magnetosphere and increase the drag by arranging multiple coils printed on a thin membrane in a deployable modular structure. To investigate the increased drag achieved by using this arrangement, a 3-D MHD analysis is performed, and the drag coefficient and the shape of the magnetosphere are compared for several different coil arrangements and distances between coils. It is found that the drag force depends on the coil arrangement and that the effect is related to changes in the structure of the magnetosphere.

Nomenclature

A = cross section of conductor

B = magnetic flux density

B_0 = representative magnetic flux density

$\boldsymbol{B}$ = magnetic flux density vector

C_d = drag coefficient

c = specific heat

d = distance between the centers of two coils

[1] Assistant Professor, Department of Mechanical Engineering, Faculty of Engineering.
[2] Professor, Department of Mechanical Engineering, Faculty of Engineering, AIAA Professional Member.

$\mathrm{d}\boldsymbol{l}$ = differential element of length of a coil

E = energy density

e = elementary electric charge

$\boldsymbol{e}_{\mathrm{c}}$ = unit vector in the direction of the current flowing through a differential element of length of a coil

$\boldsymbol{F}$ = drag vector

I = current

$\boldsymbol{I}$ = identity matrix

I_{c} = coil current

L = theoretical representative length of magnetosphere obtained using the magnetohydrodynamic approximation

l = length of conductor

m = mass

m_{i} = ion mass

n = number density

p = pressure

p_{in} = pressure of inflow plasma

p_0 = representative pressure

R = electrical resistance

R_{c} = coil radius

R_0 = representative length

r = Larmor radius

$\boldsymbol{r}$ = position vector of a mesh

$\boldsymbol{r}_{\mathrm{c}}$ = position vector of a differential element of length of a coil

$\boldsymbol{S}$ = Powell's source term

T = temperature

t = time

t_0 = representative time

u = velocity

$\boldsymbol{u}$ = velocity vector

u_{Alfven} = Alfvén velocity

$\boldsymbol{u}_{\mathrm{in}}$ = velocity vector of inflow plasma

u_0 = representative velocity

G = closed curve along a coil

γ = ratio of specific heats

μ_0 = permeability of vacuum

ρ = mass density

ρ_{in} = mass density of inflow plasma

ρ_R = electrical resistivity

ρ_0 = representative mass density

Subscripts

c = coil

in = inflow plasma

0 = representative value

I. Introduction

THE concept of a magnetic sail as a propulsion system for deep-space exploration was proposed by Zubrin and Andrews in 1991 [1]. As shown in Fig. 1, the magnetic sail is based on the same principle as the interference between the Earth's magnetic field and the solar wind plasma. The magnetic field created by a coil bends the orbit of the plasma flow and forms a magnetosphere into which the plasma flow does not enter. At the same time, an induced current is generated on the magnetopause. A bow shock is formed in front of the magnetosphere, and the momentum and pressure of the plasma are high in the magnetosheath between the bow shock and the magnetopause. The magnetic

field in front of the coil is compressed by the dynamic pressure of the plasma flow. The magnetic field behind the coil is stretched, with the formation of a magnetotail. Furthermore, a plasma sheet is formed behind the coil. Plasma accumulates in the plasma sheet, and the induced current on the magnetopause flows to the sheet [2]. When such a magnetosphere is generated, the momentum change of the plasma flow and the Lorenz force both act as drags on the coil [3].

To obtain a thrust useful for deep-space exploration, a sufficiently large magnetic moment is required. This poses a problem for construction methods, because to generate such a large moment, a superconducting coil with a radius of several kilometers is necessary. As an alternative to a coil, the E-Sail, in which a tether charged with static electricity is expanded radially, has been proposed [4,5]. In addition, because plasma drag is correlated with the size of the magnetosphere, methods based on expanding the magnetosphere generated by the coil rather than increasing the magnetic moment itself have been studied. To be specific, a mini-magnetospheric plasma propulsion (M2P2) device [6] and a ring-current magneto-plasma sail (MPS) [7] that expand the magnetosphere by injecting plasma from a spacecraft have been proposed. To expand the magnetosphere, both the M2P2 and ring-current MPS require a working fluid.

To circumvent the requirement of either a huge coil or a working fluid for the generation of large thrust, the present paper proposes a new method that uses a deployable modular structure for coil construction and arranges multiple coils printed on a thin membrane to expand the magnetosphere and increase the drag. Section II introduces the concept of a deployable modular structure, and Sec. III reports the result of a 3-D MHD analysis, as well as explaining how the magnetospheric interference due to the arrangement of two coils affects propulsion performance. Conclusions are presented in Sec. IV.

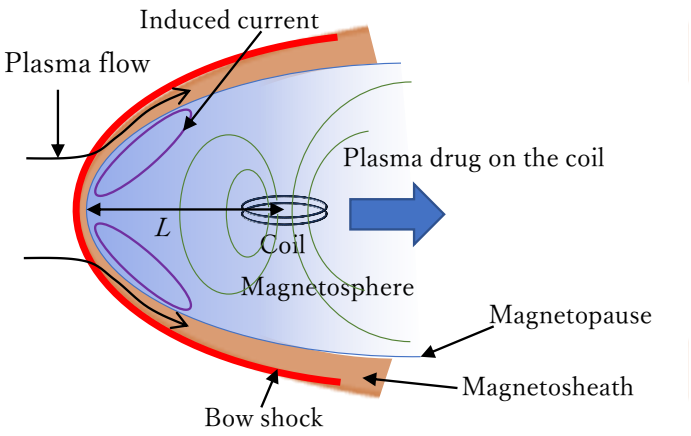

Fig. 1 Principle of magnetic sail

II. Concept of Deployable Modular Structure

Various deployable structures have been proposed for the construction of large structures for use in space that have light weight and small size at launch. The concept of a deployable membrane structure can be applied to a magnetic sail by printing the coil for the sail on a membrane as a flexible printed circuit (FPC). There are many structural approaches to the deployment of membranes such as sails in two dimensions. For its Roll-Out Solar Array (ROSA), NASA has constructed a $6\ \mathrm{m} \times 13\ \mathrm{m}$ rectangular membrane by rolling out, and Mega-ROSA, which is a modular structure equipped with multiple sheets, is being developed.[*] MegaFlex (also from NASA) has a circular membrane with a maximum diameter of 30 m. A modular structure with two MegaFlex units is being planned for mounting to various spacecraft.[*] Caltech's SSPI concept aims at constructing a huge modular structure of $3\ \mathrm{km} \times 3\ \mathrm{km}$ by in-orbit assembly. The module unit is a $60\ \mathrm{m} \times 60\ \mathrm{m}$ rectangular membrane, which is rolled out by the strain energy of triangular rollable and collapsible (TRAC) longerons [8]. Regarding the technology for mounting a membrane away from the main body of a spacecraft, several boom concepts have been proposed. In addition to basic truss deployment, there is an example of a small satellite [9] in which a deployable membrane is attached to the tip of a storable tubular extendible member (STEM). It is also possible to arrange membranes in each of the three axes using a deployable cubic modular structure. The ABLE Deployable Articulated Mast (ADAM) [10] is a modular structure in which multiple cubes of sides 1 m are connected to construct a boom with a length of 60 m. Figure 2a is a mockup of a

[*] NASA, Space Technology Mission Directorate website, https://www.nasa.gov/offices/oct/home/feature_sas.html

triangulated cylindrical origami (TCO) cubic structure with a side of 10 cm. The concept of the TCO structure is that a cylinder is stored and deployed while twisting, which is basically the same as that of ADAM. The structure in Fig. 2a has a thin membrane on which a coil is printed. For example, if the membrane coils are attached to the six sides of a cube, and four cube modules are deployed from the main body of a satellite, a modular deployable membrane coil can be constructed as shown in Fig. 2b.

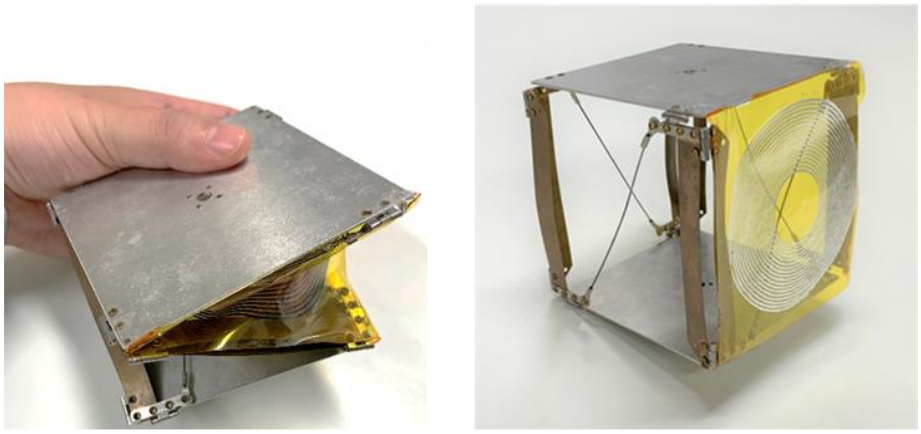

a) Stored/deployed TCO structure with a membrane coil

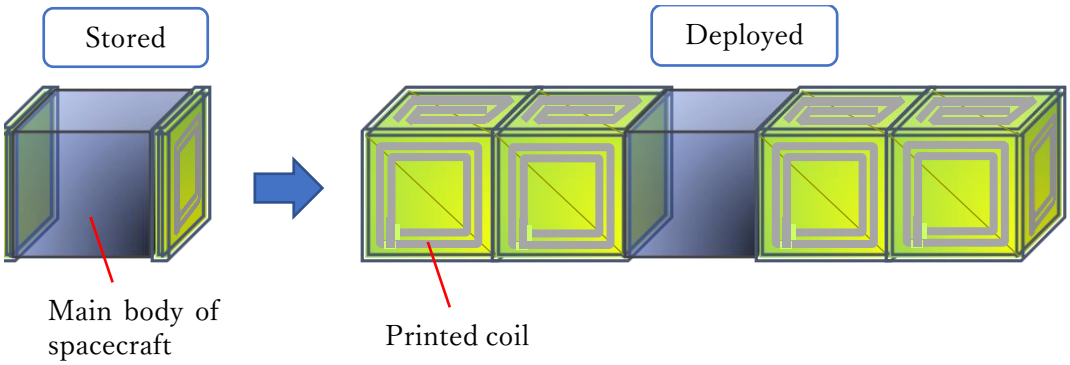

b) Concept of modular deployable membrane coils

Fig. 2 TCO structure with membrane coils.

If the modular structure concept stated above is applied to magnetic sails and magnetic plasma sails, it may be possible to find a method of expanding the magnetosphere using an arrangement of multiple coils. In fact, it has been shown experimentally that drag was increased by the use of multiple coils [11]. In addition, by mounting multiple coils, it is possible to prevent complete loss of propulsive function in the event of failure of a single coil. Therefore, this paper analyzes the relationship between coil arrangement and plasma drag. In a previous study of magnetic sails

and magnetic plasma sails using multiple coils, a 3-D MHD analysis was conducted to determine an appropriate arrangement for confining the jet plasma of an MPS [12]. In that study, the effect of confinement of the injected plasma was evaluated by combining the directions of the magnetic axes of the two magnetic dipoles.

In the case of a single coil, several previous studies have reported that the drag depends on the angle of attack of the coil [13–16]. This dependence arises from the shape of the magnetic field with respect to the plasma flow. That is, the angle of attack of the coil changes the shape of the magnetosphere, and the drag force also changes as a result. Therefore, in the present study, the behavior of the drag force is investigated by changing the direction and distance of a combination of multiple coils, because changing the direction and distance of multiple coils is equivalent to changing the shape of the magnetosphere. It is known that to expand the magnetosphere, one effective method is to arrange the coils next to each other and expand the area in which the plasma flow and the magnetic field generated by the coils collide with each other. Thus, this study examines three types of arrangement (cases A, B, and C) of two coils, as shown in Fig. 3. The distance between the centers of the coils is d. These arrangements can be realized by applying the various deployable modular structural concepts described above. Case A using magnetic dipoles has been considered previously [12], but cases B and C have never been investigated, nor have the effects of the distance d. Furthermore, the analysis presented here is for a torus-shaped coil, rather than a magnetic dipole.

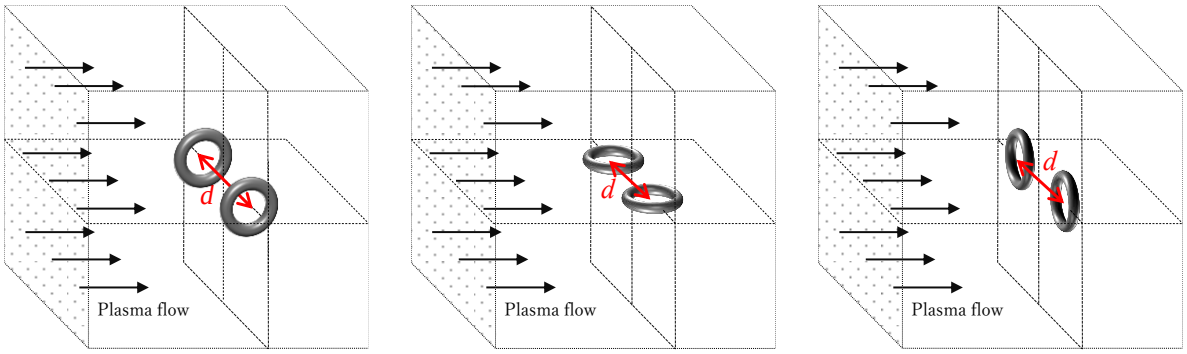

Fig. 3 Arrangements of two coils.

III. Analysis of Plasma Drag

Many analyses using either a magnetohydrodynamic (MHD) model or a particle-in-cell (PIC) model have been performed to calculate the thrusts of magnetic sails and magnetic plasma sails, with the choice of model being determined by the scale of the sail [17–20]. The computational cost of the PIC method is higher than that of the MHD method. According to the principle illustrated in Fig. 1, the orbit of a plasma particle is bent by cyclotron motion of radius r in the magnetosphere, and the particle does not enter the magnetosphere. This holds when r is sufficiently smaller than the distance L at which the plasma dynamic pressure and the coil magnetic pressure are balanced ($r \ll L$) and the approximation of an electromagnetic fluid can be applied, allowing the plasma drag to be calculated appropriately by MHD. However, when r is equal to or larger than L ($r \geq L$), the MHD approximation cannot be applied, because the plasma particles slip away through the magnetopause, and the drag due to the generation of the magnetosphere is smaller than the result obtained from MHD. In this case, the PIC method must be used to obtain an appropriate value for the drag. Furthermore, in the PIC analysis, the phenomenon of particle reflection in the mirror magnetic field near the coil is observed, and it is known that this effect increases the drag force [13,19].

A magnetic moment of 2.3×10^{12} $\mathrm{A\cdot m^2}$ is required to achieve the target thrust of 1 N for deep-space exploration [21]. Therefore, Table 1 shows the relationship between coil size, magnetic moment, and r/L for the magnetic moment under the solar wind conditions at 1 AU. Here, r is calculated as

$$r = \frac{mu}{eB} \tag{1}$$

and the representative length of the magnetosphere, L, is calculated as [17]

$$L = \left(\frac{\mu_0^2 R_{\mathrm{coil}}^2 I_{\mathrm{coil}}^2}{8\mu_0 \pi^2 n m u^2} \right)^{1/6} \tag{2}$$

With presently available deployable structure technology, a realistic size for construction is of the order of tens of meters, but this technology is at the stage where the construction of structures several kilometers in size by in-orbit assembly is a realistic aim. Therefore, in example 1 in Table 1, the coil radius is set to several tens of meters, and in example 2, the coil radius is set to several kilometers. For each coil scale, the Appendix shows the structure and power budget of a magnetic sail for deep space exploration using FPC coils and the 2-D or 3-D deployable modular structure shown in Sec. 2. As shown in the Appendix, an enormous number of launches are required to construct a sail that is capable of generating the magnetic moment required for deep space exploration. If through the use of a suitable coil

arrangement it were possible to increase the thrust by a factor of 1.1, for example, then the number of launches could be reduced by 10%, and if the thrust were increased by a factor of 1.4, then the number of launches could be reduced by 30%. The purpose of this paper is to investigate whether such increases can be achieved. As mentioned in the Appendix, the practical realization of magnetic sails using FPC coils still faces problems with regard to the number of launches, power, and presently available construction techniques, but the aim here is simply to obtain a basic understanding of the mechanism by which the positional relationship between the two coils affects the thrust, without detailed consideration of practical implementation.

As shown in Table 1, the scale involved is $r / L > 1$, and therefore a detailed parametric study of the dependence of the thrust on the positional relationship of the coils requires the use of a PIC approach. Furthermore, to reduce computational cost, this should be a 2-D analysis. On the PIC scale, where the particle behavior is dominated by that of the ions, previous studies have shown that the magnetospheric structures are qualitatively similar to those on the MHD scale, that is, a bow shock and magnetosphere are produced, a loop current is generated on the magnetopause, and a Lorentz force is generated [14,20,21]. Another previous study has demonstrated the effectiveness of multiple coils in PIC-scale experiments using coils with diameter of 30 mm [12]. By clarifying the qualitative features of the shape of magnetosphere and the drag coefficient through a 3-D MHD analysis, the present study should provide a basis for a further parametric study of a multi-coil magnetic sail using the PIC method. Although phenomena caused by the motion of plasma particles cannot be evaluated by MHD, it is possible to evaluate the macroscopic behavior of a particle group in a magnetic fluid, and important knowledge can be obtained for the behavior of particles on the PIC scale.

Table 1 Examples of coil size and *r*/*L* for a magnetic sail in the solar wind

Example	Coil radius, m	Coil current, A · turn	Magnetic moment, A · m^2	*r*/*L*
1	30	8.0×10^{8}	2.3×10^{12}	5.1
2	3.0×10^{3}	8.0×10^{4}		

A. Simulation Model

We solve the 3-D ideal MHD equation numerically to simulate the interaction between the solar wind and the magnetic field generated by the coils. In this simulation, the quasineutrality condition is adopted, the displacement current is ignored, and the electrical conductivity is assumed to be infinite. The validity of these assumptions has been

discussed in previous studies using the magnetic Reynolds number as a parameter. The ideal MHD assumption is valid for magnetic Reynolds numbers of 10 or higher [22]. The magnetic Reynolds number of the solar wind is 10^8 [23], and therefore ideal MHD can certainly be assumed in the present study. The MHD equation is [15,24]

$$\frac{\partial \boldsymbol{Q}}{\partial t} + \nabla \cdot \boldsymbol{F} = \boldsymbol{S} \tag{3}$$

where

$$\boldsymbol{Q} = \begin{bmatrix} \rho \\ \rho \boldsymbol{u} \\ \boldsymbol{B} \\ E \end{bmatrix}, \quad \boldsymbol{F} = \begin{bmatrix} \rho \boldsymbol{u} \\ \rho \boldsymbol{u}\boldsymbol{u} + \left(p + \dfrac{\boldsymbol{B} \cdot \boldsymbol{B}}{2} \right) \boldsymbol{I} - \boldsymbol{B}\boldsymbol{B} \\ \boldsymbol{u}\boldsymbol{B} - \boldsymbol{B}\boldsymbol{u} \\ \left(E + p + \dfrac{\boldsymbol{B} \cdot \boldsymbol{B}}{2} \right) \boldsymbol{u} - \boldsymbol{B}\left(\boldsymbol{B} \cdot \boldsymbol{u} \right) \end{bmatrix}, \quad \boldsymbol{S} = -\nabla \cdot \boldsymbol{B} \begin{bmatrix} 0 \\ \boldsymbol{B} \\ \boldsymbol{u} \\ \boldsymbol{B} \cdot \boldsymbol{u} \end{bmatrix}$$
$$E = \frac{\rho \boldsymbol{u} \cdot \boldsymbol{u}}{2} + \frac{p}{\gamma - 1} + \frac{\boldsymbol{B} \cdot \boldsymbol{B}}{2} \tag{4}$$

This MHD equation is solved in an eight-wave formulation [24,25]. The total variation diminishing (TVD)–Lax–Friedrichs scheme is used for solving the differential equations. The MUSCL method using the MINMOD function is used for higher-order accuracy. The time integral is second-order precision.

The reliability of our code is confirmed by solving 1-D MHD equations for the Riemann problem [14,26]. This method is widely used to test schemes for ideal MHD. The following state quantities are given as an initial condition, and the transient response is observed:

$$\left(\rho,\ p,\ u_x,\ u_y,\ u_z,\ B_x,\ B_y,\ B_z \right) = \begin{cases} \left(1.0,\ 1.0,\ 0,\ 0,\ 0,\ 0.75,\ 1.0,\ 0 \right) & \text{for } x \le 0.5 \\ \left(0.125,\ 0.1,\ 0,\ 0,\ 0,\ 0.75,\ -1.0,\ 0 \right) & \text{for } x > 0.5 \end{cases} \tag{5}$$

The calculation conditions are γ = 5/3 and a grid number of 800. Figure 4 shows the results when t = 80. It can be observed that a fast expansion wave ($x < 0.4$), a slow compound wave ($x \approx 0.47$), a contact discontinuity ($x \approx 0.55$), a slow shock wave ($x \approx 0.63$), and a fast expansion wave ($x > 0.65$) are formed. A calculation under the same conditions was verified by Ryu and Jones [27], and our results shown in Fig. 4 are in good agreement with theirs. Hence, the reliability of our code is confirmed.

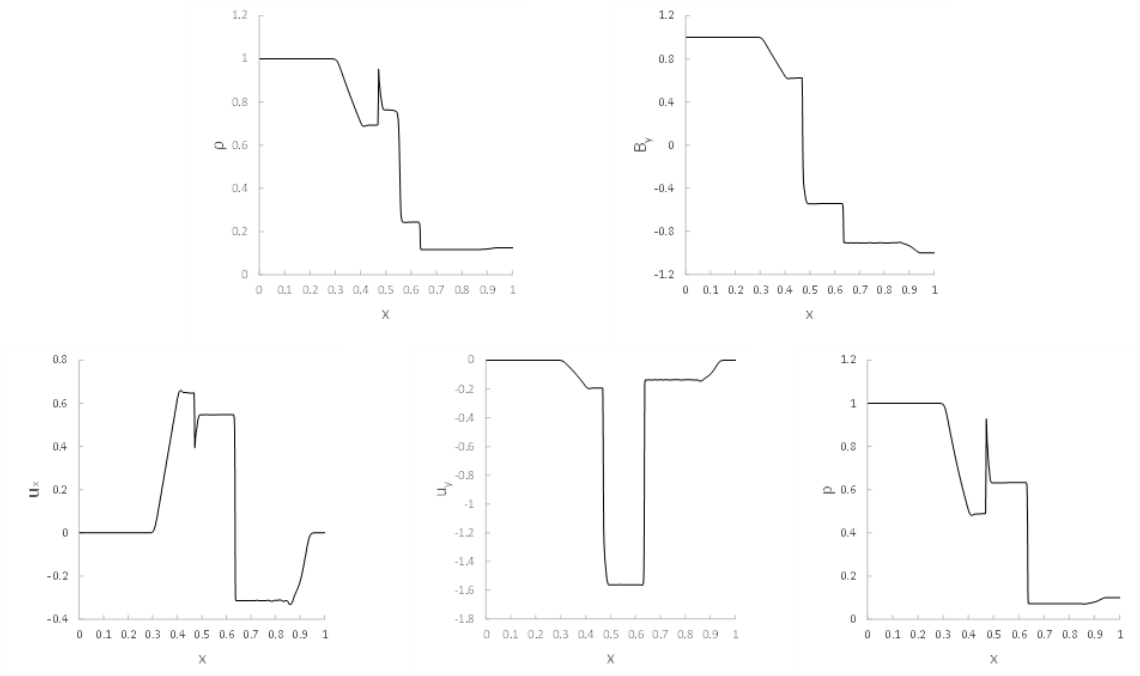

Fig. 4 Results of MHD analysis for Riemann problem.

B. Calculation Conditions

The analysis space is set as shown in Fig. 5. It is mesh-divided into orthogonal grids with a grid width of $\Delta x = \Delta y = \Delta z = 0.05R_c$. The number of meshes is 140 in the *x* direction, 320 in the *y* direction, and 320 in the *z* direction. The center of the coil is placed in the planes *x* = 50 and *z* = 160. The plane *x* = 0 is set as the plasma inflow plane, and the inflow plasma is set to correspond to the conditions of the solar wind at 1 AU, as shown in Table 2 [14,15]. Monovalent ions are assumed in this analysis. Initially, the analysis space is filled with the static plasma shown in Table 2. The diameter of the coil cross section is set to $0.3R_c$. The boundary conditions of the coil surface are given by fixing all physical quantities within $0.3R_c$ from the center of the cross section of the coil [16]. The magnetic field is calculated according to the Biot–Savart law [15]:

$$\boldsymbol{B}(\boldsymbol{r}) = \frac{\mu_0}{4\pi} I_c \int_G \frac{\boldsymbol{e}_c \times (\boldsymbol{r} - \boldsymbol{r}_c)}{|\boldsymbol{r} - \boldsymbol{r}_c|^3} \mathrm{d}l \tag{6}$$

The value of the magnetic moment of the coil affects the size of the magnetosphere in the analysis space and is determined by the coil current and coil radius. In this analysis, the ratio between the coil current and the coil radius,

I_c / R_c [A · turn/m], is set to 0.15, whereby, from Eq. (2), the representative length of the magnetosphere L is $1.2R_c$ (24 mesh) for a single coil and $1.5R_c$ (30 mesh) when the two coils are arranged at d = 0. Because the coil radius is 20 mesh and the coil center is at $(x, y, z) = (50,160,160)$, L can be accommodated in the analysis space and can be set to be larger than the coil radius by setting I_c / R_c to 0.15. The analysis is performed with nondimensional quantities. Table 3 shows the parameters and the corresponding quantities used for nondimensionalization.

The plasma drag is calculated as follows based on the momentum balance with respect to the control volume in the analysis space when it has reached a steady state after a sufficient time has elapsed, as shown in Fig. 6 [3]:

$$\boldsymbol{F} = -\oint_S (\rho \boldsymbol{u}\boldsymbol{u} + p\boldsymbol{I}) \cdot \boldsymbol{n}_s \, \mathrm{d}S - \oint_S \left(\frac{\boldsymbol{B} \cdot \boldsymbol{B}}{2} \boldsymbol{I} + \boldsymbol{B}\boldsymbol{B} \right) \cdot \boldsymbol{n}_s \, \mathrm{d}S \tag{7}$$

$$C_\mathrm{d} = \frac{F_x}{\rho_\mathrm{in} \boldsymbol{u}_\mathrm{in}^2 \pi R_c^2 / 2} \tag{8}$$

Table 4 shows these analysis conditions in terms of physical quantities with their units. Because the analysis is performed with nondimensional quantities, the transient response and the drag coefficient are the same in examples 1 and 2, but the drag is different. In example 2, the coil radius is reduced to 1/10 of its value in example 1, and so the drag force is reduced by a factor of 1/100, but the MHD scale is larger than in example 1, depending on the ratio r / L. However, as mentioned above, the MHD scale is not the scale of an actual spacecraft, and so the drag value itself has no significant meaning in this study. Therefore, the comparative evaluation here is performed in terms of the drag coefficient C_d.

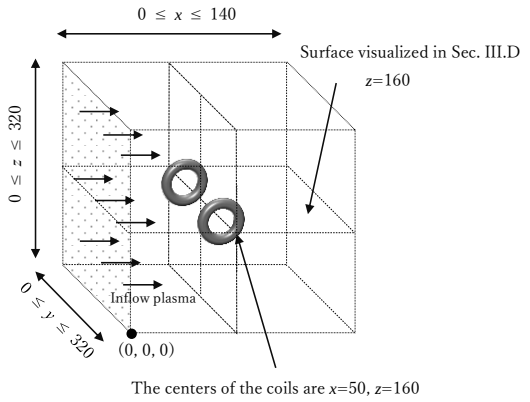

Fig. 5 Definition of calculation area

Table 2 Specifications for analysis

		Value	Nondimensional value
Inflow plasma	ρ_{in}	$5m_{\mathrm{i}}\times10^{6}$ kg/m^3	5
	u_{in}	400 km/s	0.917
	p_{in}	20 eV	8.68×10^{-2}
	$\boldsymbol{B}_{\mathrm{in}}$	0	0
Initial state	ρ	—	$B^2/u_{\mathrm{Alfven}}^2$ ($u_{\mathrm{Alfven}}=700$ km/s)
	u	—	0
	p	—	0.1
	$\boldsymbol{B}$	—	Generated by coils
	I_{c}	$0.15R_{\mathrm{c}}$ [A · turn]	—

Table 3 Representative parameters for nondimensionalization

Representative parameter	Value used for nondimensionalization
R_0	$2R_{\mathrm{c}}$ [m]
B_0	2×10^{-8} T
ρ_0	$m_{\mathrm{i}}\times10^{6}$ kg/m^3
u_0	$B_0/\sqrt{\mu_0\rho_0}$
t_0	R_0/u_0
p_0	$\rho_0 u_0^2$

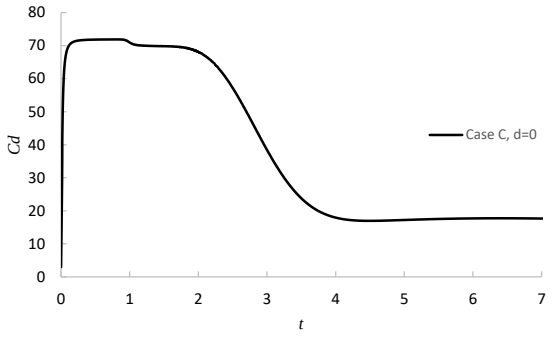

Fig. 6 Transient response of drag coefficient

Table 4 Correspondence of nondimensional analysis conditions to physical quantities and their units

Example	Coil radius, m	Coil current, A · turn	Magnetic moment, A · m^2	r/L
1	1×10^5	1.5×10^4	4.7×10^{14}	0.86
2	1×10^4	1.5×10^3	4.7×10^{11}	8.6

C. Validation of Simulation for Interaction between Solar Wind and Magnetic Field from a Coil

To evaluate the validity of our analysis, the physical quantities around the magnetosphere obtained from analyses for a single coil are visualized in 3-D, and we check whether the results agree with the magnetospheric structures found in previous research on the Earth's magnetosphere and in MHD analyses [2,15,16]. Figure 7 shows the states of the magnetosphere and the plasma flow for a single coil when the coils are placed parallel to the inflow plasma (cases A and B) and vertical to it (case C). The color contours in Fig. 7a show the momentum distribution, and the black lines are the streamlines. The color contours in Fig. 7b show the pressure distribution, and the black lines are the magnetic force lines. The color contours in Fig. 7c show the induced current distribution, and the black lines are the current paths. The color contour diagrams are in the planes $y = 160$ and $z = 160$.

First, it can be seen from Fig. 7a that a bow shock and magnetosheath, both of which are high-momentum regions, are formed, and a magnetosphere is formed inside them. The streamlines change their orbits in the magnetosheath and do not enter the magnetosphere. The momentum is almost zero in the magnetosphere. In Fig. 7b, the formation of the bow shock and magnetosheath, both of which are also high-pressure regions, is confirmed by the pressure distribution, and it can be seen that the magnetic force lines are compressed in front of the coil and stretched at its rear, thereby forming a magnetotail. The induced current distribution in Fig. 7c confirms that the induced current increases near the magnetopause. For the arrangements with the coil parallel to the inflow (cases A and B) in Fig. 7c, it can be seen that a plasma sheet is formed behind the coil, similar to the Earth's magnetic field structure. The fact that the induced current near the magnetopause appears as two layers is caused by changes in the magnetic field in front of the coil and in the magnetic field behind the coil across the cusp. In the case of a coil placed vertical to the inflow (case C), the current path in Fig. 7c reveals that multiple current loops are formed near the magnetopause. For coil arrangements parallel to the inflow (cases A and B), Fig. 7c shows that multiple current loops are generated near the magnetopause in front of the coil, and meanwhile the current loop behind the coil flows from the magnetopause to the plasma sheet. This is again similar to the Earth's magnetic field structure. The current path in the region $z < 160$ has a shape that is

symmetrical with that in the region $z > 160$. These results are in good agreement with those of previous studies [2,15,16]. Thus, the validity of our simulations of the interaction between the solar wind and the magnetic fields generated by the coils is confirmed.

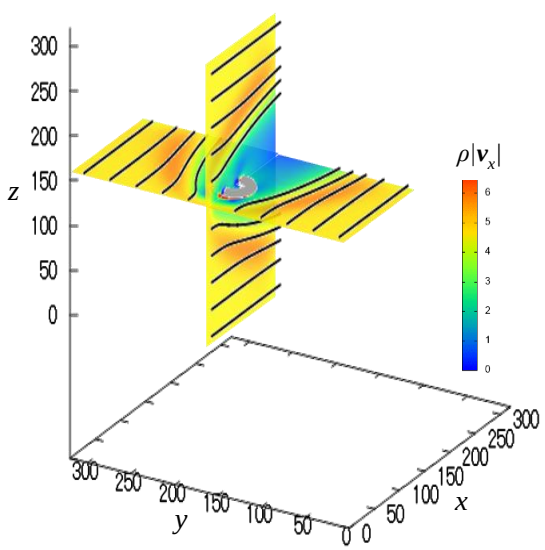

Parallel coil (cases A and B)

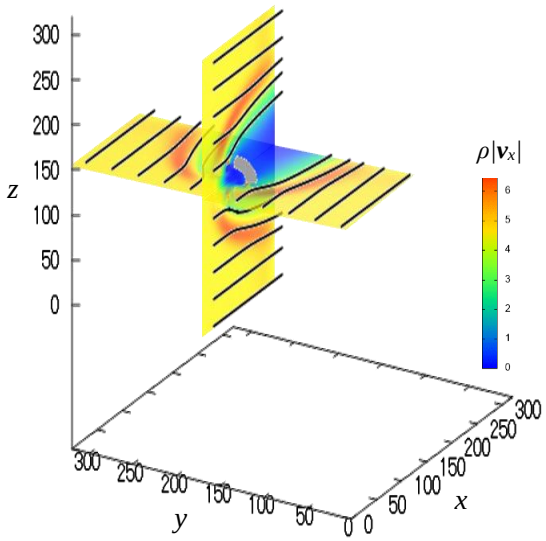

Vertical coil (case C)

a) Momentum distribution and streamlines

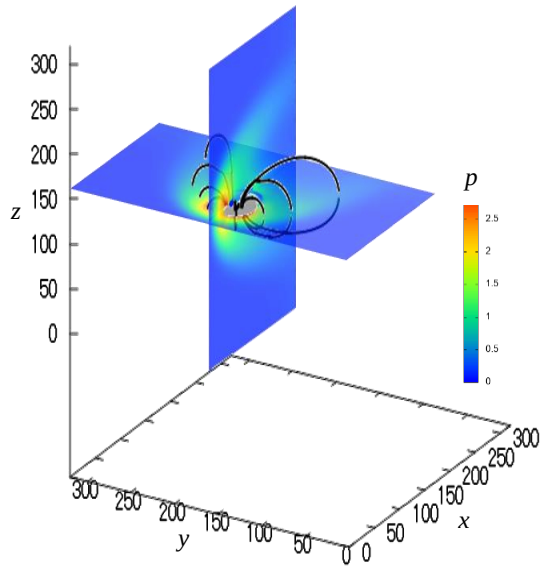

Parallel coil (cases A and B)

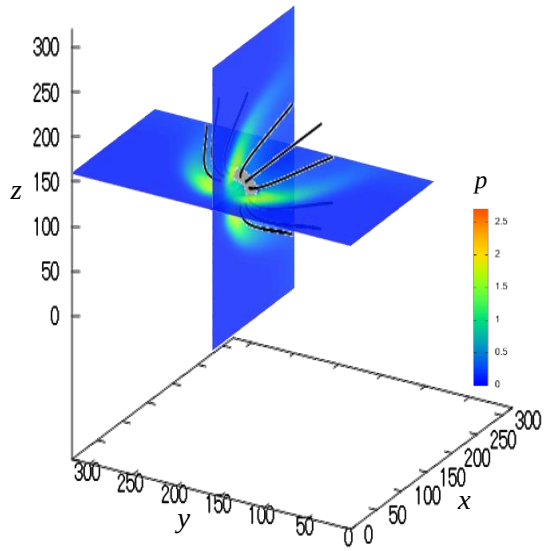

Vertical coil (case C)

b) Pressure distribution and magnetic force lines

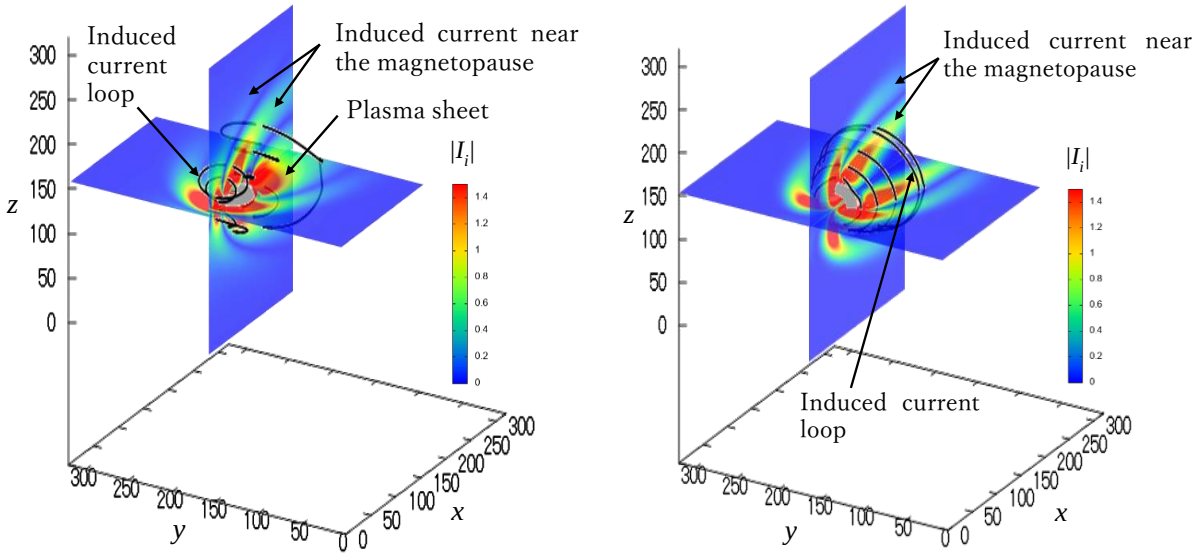

Parallel coil (cases A and B) Vertical coil (case C)

c) Induced current distribution and current path

Fig. 7 State of magnetosphere and plasma flow.

D. Comparison with Regard to Coil Arrangement

For cases A, B, and C shown in Fig. 3, simulations were conducted under the conditions d = 0, 40, 80, 120, and 160 mesh, and the results are compared. The radius of the coil is 20 mesh. The circumferential direction of the current flowing through the two coils is the same. Figure 8 shows the drag coefficient in each case. Figure 9 shows the momentum distribution on the visualized surface with z = 160 defined in Fig. 5. The coil is marked in black.

For d = 0, the drag coefficient in case C, where the coil is perpendicular to the flow, is about 1.5 times larger than those in cases A and B. Because this is the same trend found in previous studies [15,16], it can be concluded that the drag calculation here is correct. In each case, the drag coefficient peaks at d = 80 and then decreases. The results show that there is an optimum distance d for which the drag force can be increased most effectively owing to the influence of the magnetosheath. This optimum distance depends on the value of the magnetic moment and the coil radius, that is, it depends on the ratio I_c / R_c defined in Sec. III.B. Under the condition I_c / R_c = 0.15 [A·turn/m] set in this analysis, the drag force can be increased most effectively when the distance is about four times the coil radius. As the distance between the coils increases, the magnetosheath, which has a high momentum, as shown in red in Fig. 9, penetrates between the coils, deforming the magnetosphere and making it narrow behind the coils. The decrease in

C_d after d = 80 can be attributed to this effect. The deformation of the magnetosphere in front of the coil is most prominent in case B, as can be seen from the area surrounded by the dashed line in Fig. 9b at d = 120.

In all cases, magnetosheath interference is absent up to d = 40, and there is no expansion of the magnetosphere at x = 140. However, the area of low momentum (shown in blue) in the magnetosphere is increased compared with that at d = 0, which can be considered to contribute to the increase in C_d from d = 0 to d = 40. From a comparison of the momentum distributions at d = 40 and d = 80 in each case, it can be seen that not only has the magnetosphere at x = 140 expanded but also the influence of the penetration of the magnetosheath between the coils has begun to appear, although there is only a slight increase in C_d from d = 40 to d = 80.

When comparing the effects of interference by the magnetosheath behind the coil, it should be noted that in case B, the plasma sheet behind the coil has a strong influence, and therefore the interference by the magnetosheath is difficult to judge from Fig. 9b. Accordingly, cases A and C alone are compared from here on. Within the areas surrounded by the dashed lines at d = 80 in Figs. 9a and 9c, the part in green reaches farther toward the rear in case C than in case A. That is, in case C, the penetration by the magnetosheath is more likely to affect the region farther behind the coil. As shown in Fig. 7b, the magnetic force lines of case C have a large component in the x direction (i.e., the direction of plasma flow), and so it can be concluded that the plasma more easily penetrates far behind the coil. Given that case B has this magnetic field structure, it is not surprising that the fluctuations in the value of C_d are small.

Comparing the areas surrounded by the dashed line at d = 120, it can be seen that the red part reaches farther toward the rear in case A than in case C, indicating that the areas of magnetosheath interference easily reaches behind the coil in case A. The reason why the magnetosheath suddenly penetrates backward at d = 120 in case A is that there is a point between the coils at which the magnetic field component orthogonal to the plasma flow becomes zero, as shown in Fig. 10. It can thus be concluded that the plasma flow more easily penetrates the region beyond that point.

In this analysis, a current of $0.15R_c$ is passed for each coil. Therefore, from Eq. (6), when d = 0, this is the same situation as when a current of $0.3R_c$ is passed through a single coil. Therefore, in all cases, if the total coil current is the same, then a combination of multiple coils can provide a greater drag force than a single coil. Thus, it is indeed possible to increase the plasma drag by using an appropriate coil arrangement. Under the condition I_c / R_c = 0.15 $[\mathrm{A \cdot turn/m}]$ set in this analysis, compared with C_d for d = 0, the greatest increase in drag coefficient is obtained in case A and the smallest increase in case C. That is, the effect of the coil arrangement on the increase in drag is greatest

for the arrangement in case A when the distance between the coils is four times the coil radius. The drag coefficient itself attains its maximum value when the distance is four times the coil radius in the arrangement in case C. However, the drag force becomes less than that for $d = 0$ if d is too large, because the magnetosheath interference region behind the coil then has the effect of narrowing the magnetosphere.

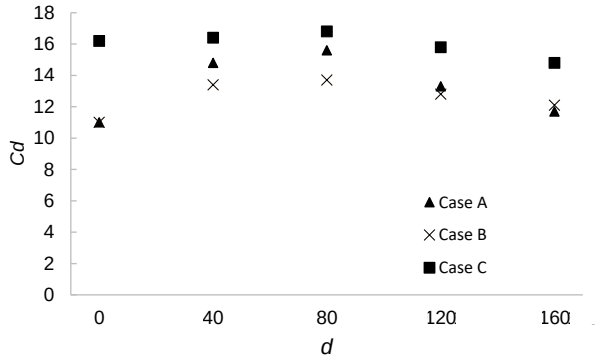

Fig. 8 Drag coefficient in cases A, B, and C.

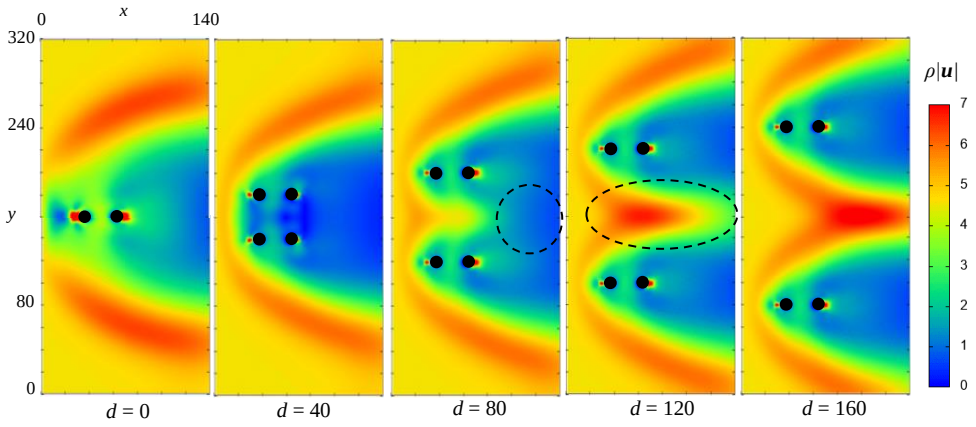

a) Case A

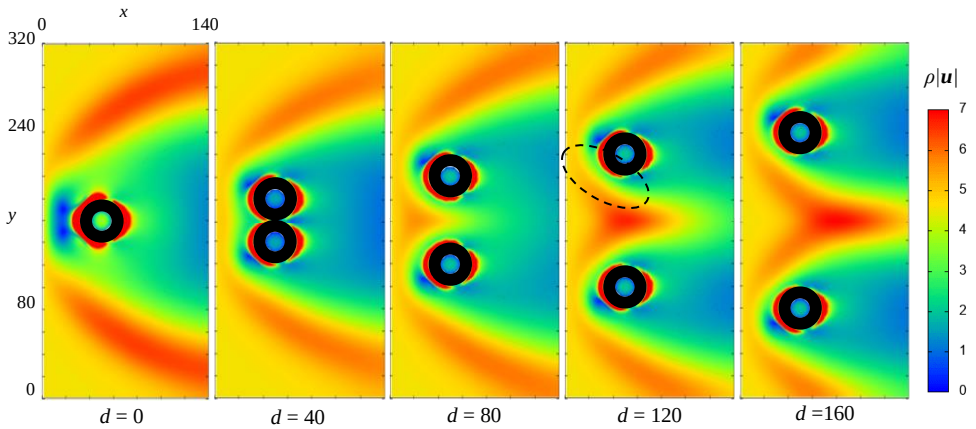

b) Case B

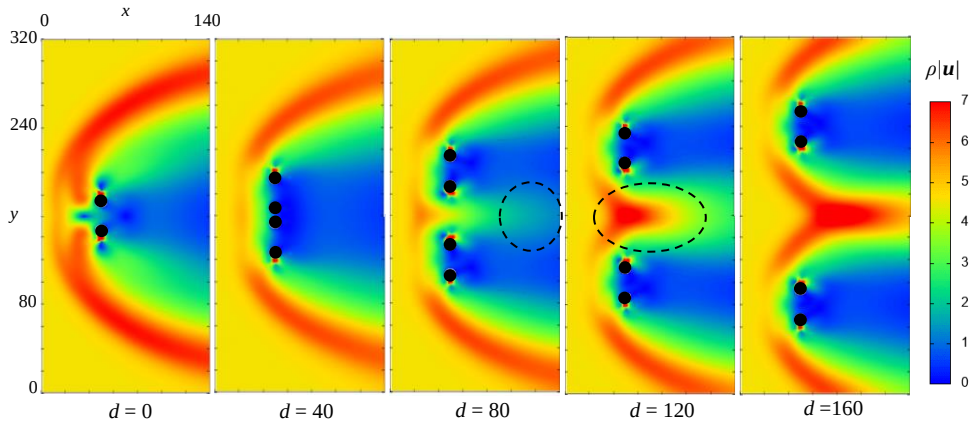

c) Case C

Fig. 9 Momentum distribution in each case.

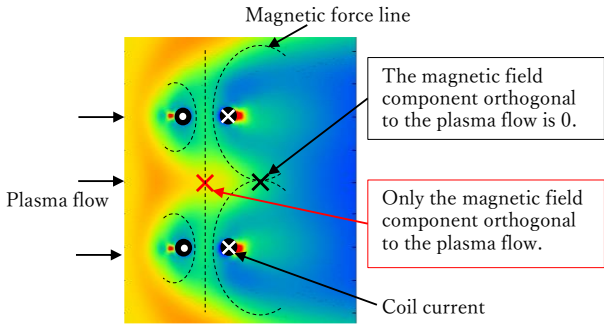

Fig. 10 Direction of magnetic field lines between coils in case A.

IV. Conclusions

In this study, we performed a 3-D MHD analysis to investigate the expansion of the magnetosphere of a magnetic sail and the increased drag obtained by appropriate arrangement of multiple coils constructed using a deployable modular structure. The conclusions of the study can be summarized as follows:

1) For the same total coil current, the results show that a combination of multiple coils can provide a greater drag force than a single coil.

2) There is an optimum distance d for which the drag force can be increased most effectively owing to the influence of the magnetosheath. This optimum distance depends on the value of the magnetic moment and the coil radius. Under the condition $I_c / R_c = 0.15\ [\mathrm{A \cdot turn/m}]$ set in this analysis, regardless of the direction of the magnetic axis of the coils with respect to the plasma flow, the drag force can be increased most

effectively when the distance between coil centers is about four times the coil radius. The drag-increasing effect of the coil arrangement is greatest when coils in the arrangement of case A are separated by four times their radius. The drag coefficient reaches its maximum value when coils in the arrangement of case C are separated by four times their radius.

3) As the distance between coils increases, the magnetosheath penetrates between the coils, deforming the magnetosphere, narrowing it behind the coils, and reducing the drag.
4) The region of magnetosheath interference tends to penetrate to the rear of the coil if the direction of the magnetic force lines is the same as that of the plasma flow.

In this paper, a basic study of a configuration with two coils has been conducted. However, practical realization of a magnetic sail system capable of providing sufficient thrust for deep space exploration and based on a deployable structure incorporating only two FPC coils faces a number of challenges. In particular, a system using only two coils would require them to be of a size and weight such that construction in a single launch would be difficult with current technology. It is therefore important to consider the possibility of a magnetic sail system based on a multi-coil system that is capable of providing efficient drag by assembling a large number of small deployable coils. With this in mind, future work will aim at predicting the thrust of a multi-coil system through an appropriate extrapolation of the results of the MHD analysis conducted in this paper.

Appendix: Feasibility of Magnetic Sail Construction by Using a Deployable Membrane Structure

Table A1 shows the budget in terms of the number of coil turns, weight, power, temperature, number of launches, and size for the construction of a magnetic sail with a deployable structure that generates a magnetic moment of $2.3\times10^{12}\ \mathrm{A\cdot m^2}$ suitable for deep space exploration, which is the subject of the analysis in this paper. The coil in Table A1 requires wiring in orbit after the FPC sheets have been deployed and assembled. Assuming an eight-layered FPC that can be created with current technology, a copper wire with a thickness of 70 μm is used for the calculation. In Table A1, “Total number of coil turns” refers to the number of coil loops that the magnetic sail requires in total. Thus, the magnetic sail considered here requires 15 000 turns to provide the required magnetic moment. In the SSPI structure shown in Fig. A1, 400 wire elements can be printed on a single layer of an FPC sheet, and therefore, through the use of electrical connections to adjacent FPC sheets to form a coil loop, 400 turns can be printed on a single layer

of an FPC. On an eight-layered FPC sheet, 3200 turns can be printed. Therefore, 16 000 turns can be obtained by overlaying five FPC sheets. By electrically connecting the single closed loops of the coil as described by “Connection between coil turns and applied voltage” in Table A1 and applying the voltage, a current determined by the conductor resistance of the wire flows. The conductor resistance of the wire is calculated from its cross-sectional area and length and the electrical conductivity of copper, and the power consumption is calculated as the product of the current and the applied voltage. No external resistor is added. The number of launches is calculated from the total weight of the conductor. The coil weight is calculated from the volume and density of the conductor, and the weight that can be launched at one time is set to 15 000 kg. The weight is calculated from the weight of the wire alone, without including that of the base film of the FPC sheet. The rise in temperature of the wire due to the flow of current is calculated as follows:

$$\Delta T = \frac{I^2 R t}{mc} \tag{A1}$$

where

$$R = \frac{\rho_R l}{A} \tag{A2}$$

Figure A1 shows examples of structural concepts in which multiple large coils of diameter 3 km with the design parameters listed in Table A1 are constructed using FPC sheets. The SSPI structure, which is a 2-D deployable structure with a large surface area, and the TCO structure, which is a 3-D deployable structure with a high degree of freedom of FPC placement on each surface of the three axes, are considered in the present budget. In the analysis carried out in this paper, a toroidal coil is considered, which differs in cross-sectional shape from a printed coil, for which the line width is large with respect to the thickness. Additionally, although the coil in Fig. A1 has a polygonal shape, it is actually possible to fabricate a coil that is closer to circular by shape printing and using a combination of structural modules. The effects of the difference in shape between a realistic printed coil and the toroidal coil considered in the simulation on the results obtained need to be investigated in the future.

The structural concepts in Fig. A1 can be arranged in the form of a single coil by overlaying the FPC sheets, or they can be arranged like multiple coils without overlaying the sheets. The magnetic moment in Table A1 is calculated by stacking all the FPC coils as a single coil, but if the coils are separated into two wings as in the SSPI structure in Fig. A11, the magnetic moment of a single wing is then $1.15\times10^{12}\ \mathrm{A\cdot m^2}$ and r/L of a single wing is 6.3. The latter

does not represent a significant difference in the analysis scale compared with $r/L = 5.1$ at a magnetic moment of $2.3\times10^{12}\ \mathrm{A\cdot m^2}$. Regarding the power consumption, dividing the required power by the surface area of the assembled structure gives $154\ \mathrm{W/m^2}$ and $909\ \mathrm{W/m^2}$, respectively, for the SSPI and TCO structures shown in Fig. A1. Compared with the $250\ \mathrm{W/m^2}$ of Mega Flex, these can be considered to be realistic values, but since that of the TCO structure exceeds $250\ \mathrm{W/m^2}$, it is necessary to adopt a design such that solar cells are placed even in locations where there is no coil. The temperature rise during 10 s operation is slight owing to the high mass of the wire. If a superconducting material were used instead of copper, the magnetic moment per coil could be increased, but there are technological problems with printing superconducting materials on an FPC because these materials are brittle and therefore usually difficult to fold. However, a method has been proposed in in which a kirigami structure is used that allows a printed wire to be folded without creases,* which offers a possible solution to this problem. With current technology, integral molding of an FPC harness is possible up to 100 m.**

By laying down small FPC coils as shown in Fig. A2, it should be possible to construct a multi-coil magnetic sail using in-orbit assembly without the need for in-orbit wiring. However, the resulting configuration differs greatly from that considered in this paper, and so another analytical model with appropriate conditions will need to be developed for the evaluation of this approach.

Table A1 Structural and electrical budget for a magnetic sail using FPC coils (Fig. A1)

Electrical resistivity of copper	$1.68\times10^{-8}\ \Omega\cdot\mathrm{m}$
Specific heat of copper	$400\ \mathrm{J/(kg\cdot K)}$
Density of copper	$8900\ \mathrm{kg/m^3}$
Outer radius of coil	1500 m
Line width of coil	0.1 m
Thickness of wire	70×10^{-6} m
Total number of coil turns	15 000
Total mass of conductor	8.75×10^{6} kg
Connection between coil turns and applied voltage	15 000 parallel, 500 V
Total power consumption	1.7×10^{5} kW
Temperature rise (for 10 s)	0.5 K

* https://www.elephantech.co.jp/pickups/tomoe-type-kirigami-structure/
** https://www.okidensen.co.jp/jp/news/2009/release_090602.html

Number of launches	587
Size of structure as a whole	Square with sides 3 km
Magnetic moment per eight-layered FPC	$4.6\times10^{11}\ \mathrm{A\cdot m^2}$ (SSPI)
r / L per eight-layered FPC	8.72

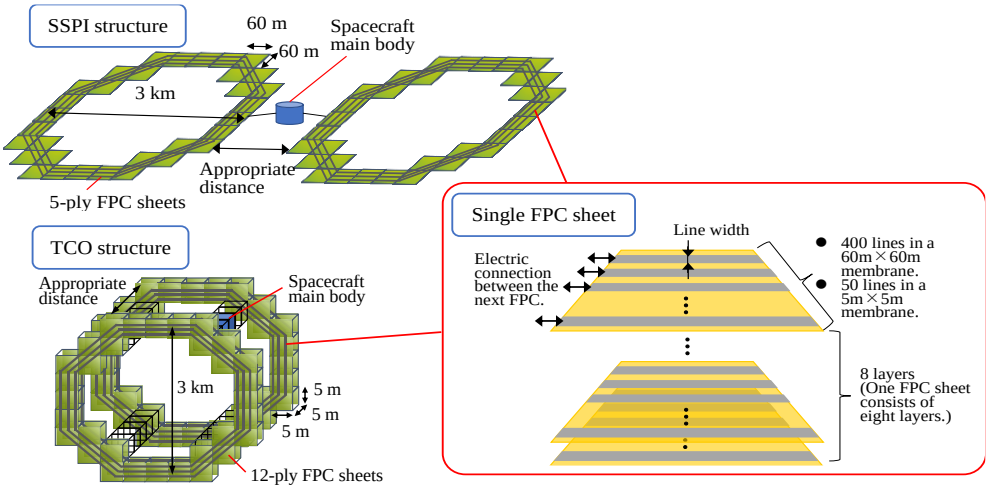

Fig. A1 Structural concept of multi-coil magnetic sails using coils of diameter 3 km.

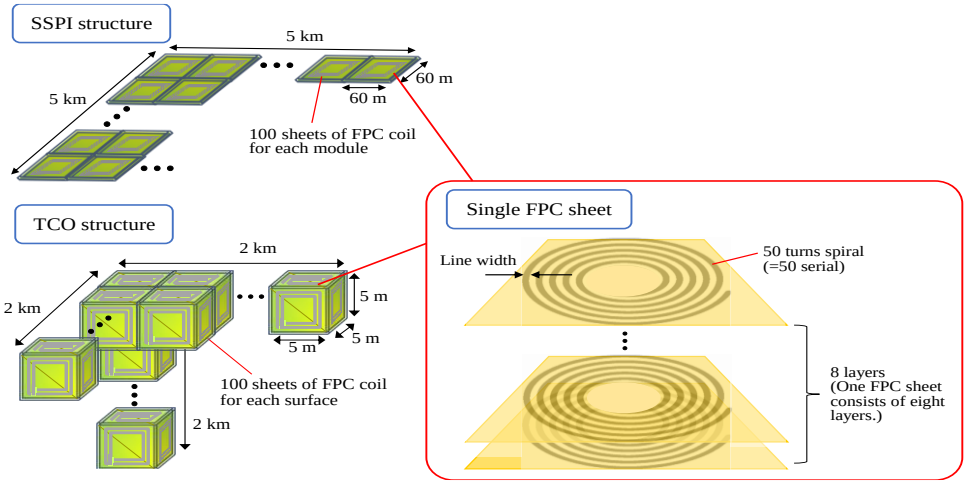

Fig. A2 Structural concept of multi-coil magnetic sails using small coils.

Funding Sources

This work was supported by JSPS KAKENHI Grant No. 19K15208.

Acknowledgments

We gratefully acknowledge communications and support from the MPS Group students in the Funaki Laboratory, working with the Yamagiwa Laboratory.

References

[1] Zubrin, R. M., and Andrews, D. G., "Magnetic Sails and Interplanetary Travel," *Journal of Spacecraft and Rockets*, Vol. 28, No. 2, Mar. 1991, pp. 197–203.
https://doi.org/10.2514/3.26230

[2] Baumjohnn, W., and Treumann, R., *Basic Space Plasma Physics*, Imperial College Press, London, 1996, pp. 1–10.
https://doi.org/10.1142/p015

[3] Nishida, H., Funaki, I., Inatani, Y., and Kusano, K., "MHD Flow Field and Momentum Transfer Process of Magneto-Plasma Sail," *Journal of Plasma and Fusion Research*, Vol. 8, 1 Sep. 2009, pp. 1574–1579.

[4] Janhunen, P., and Sandroos, A., "Simulation Study of solar Wind Push on a Charged Wire: Basis of Solar Wind Electric Sail Propulsion," *Annales Geophysicae*, Vol. 25, No. 3, Mar. 2007, pp. 755–767.
https://doi.org/10.5194/angeo-25-755-2007

[5] Mengali, G., Quarta, A. A., and Janhunen, P., "Electric Sail Performance Analysis," *Journal of Spacecraft and Rockets*, vol. 45, No. 1, Jan. 2008, pp. 122–129.
https://doi.org/10.2514/1.31769

[6] Winglee, R. M., Slough, J., Ziemba, T., and Goodson, A., "Mini-Magnetospheric Plasma Propulsion: Tapping the Energy of the Solar Wind for Spacecraft Propulsion," *Journal of Geophysical Research*, Vol. 105, No. A9, Sep. 2000, pp. 21067–21077.
https://doi.org/10.1029/1999JA000334

[7] Yamakawa, H., Funaki, I., Nakayama, Y., Fujita, K., Ogawa, H., Nonaka, S., Kunlnaka, H., Sawai, S., Nishida, H., Asahi, R., Otsu, H., and Nakashima, H., "Magneto-Plasma Sail: An Engineering Satellite Concept and its Application for Outer Planet Missions," *Acta Astronautica*, Vol. 59, Nos. 8–11, 2006, pp. 777–784.
https://doi.org/10.1016/j.actaastro.2005.07.003

[8] Royer, F., and Pellegrino, S., "Ultralight Ladder-Type Coilable Space Structures," *2018 AIAA Spacecraft Structures Conference*, AIAA 2018-1200, Kissimmee, Florida, 2018, pp. 1–14.
https://doi.org/10.2514/6.2018-1200

[9] Nakanishi, H., Sakamoto, H., Furuya, H., Yamazaki, M., Miyazaki, Y., Watanabe, A., Watanabe, K., Torisakakayaba, A., and Oda, M., "Development of Nano-Satellite OrigamiSat-1 with Highly Functional Deployable Membrane," *The 4th International Symposium on Solar Sailing*, Kyoto, 2017, pp. 1–4.

[10] Douglas. M., V., “Module for an Articulated Stowable and Deployable Mast,” U.S. Patent 5267424, 1993.

[11] Ueno, K., Horie, M., Oshio, Y., and Funaki, I., “Thrust Measurement of Multi-Coils Magnetic Sail in Laboratory Experiment,” *The 60th Space Sciences and Technology Conference*, JSASS-2016-4653, Hakodate, 2016.

[12] Baba, T., Nishida, H., and Funaki, I., “Numerical Analysis Investigation of the Coil Position for Thrust Enhancement of the Multipole-Type Magneto Plasma Sail,” *The 58th Space Sciences and Technology Conference*, JSASS-2014-4250, Nagasaki, 2014.

[13] Kawashima, R., Bak, J., Matsuzawa, S., and Inamori, T., “Particle Simulation of Plasma Drag Force Generation in the Magnetic Plasma Deorbit,” *Journal of Spacecraft and Rockets*, Vol. 55, No. 5, Sep. 2018, pp. 1074–1082. https://doi.org/10.2514/1.A34040

[14] Nishida, H., Ogawa, H., Funaki, I., Fujita, K., Yamakawa, H., and Nakayama, Y., “Two-Dimensional Magnetohydrodynamic Simulation of a Magnetic Sail,” *Journal of Spacecraft and Rockets*, Vol. 43, No. 3, May 2006, pp. 667–672. https://doi.org/10.2514/1.15717

[15] Nishida, H., Ogawa, H., Funaki, I., and Inatani, Y., “Three-Dimensional Magnetohydrodynamic Simulation of Magnetic Sail,” *Journal of the Japan Society for Aeronautical and Space Sciences*, Vol. 55, No. 644, 2007, pp. 453–457. https://doi.org/10.2322/ jjsass.55.453

[16] Kajimura, Y., Funaki, I., Matsumoto, M., Shinohara, I., Usui, H., and Yamakawa, H., “Thrust and Attitude Evaluation of Magnetic Sail by Three-Dimensional Hybrid Particle-in-Cell Code,” *Journal of Propulsion and Power*, Vol. 28, No. 3, May 2012, pp. 652–663. https://doi.org/10.2514/1.B34334

[17] Funaki, I., Kojima, H., Yamakawa, H., Nakayama, Y., and Shimizu, Y., “Laboratory Experiment of Plasma Flow Around Magnetic Sail,” *Astrophysics and Space Science*, Vol. 307, Nos. 1–3, Jan. 2007, pp. 63–68. https://doi.org/10.1007/978-1-4020-6055-7_12

[18] Fujita, K., “Particle Simulation of Moderately-Sized Magnetic Sails,” *Journal of Space Technology and Science*, Vol. 20, No. 2, 2004, pp.26–31. https://doi.org/10.11230/jsts.20.2_26

[19] Ashida, Y., Funaki, I., Yamakawa, H., Usui, H., Kajimura, Y., and Kojima, H., “Two-Dimensional Particle-In-Cell Simulation of Magnetic Sails,” *Journal of Propulsion and Power*, Vol. 30, No. 1, Jan. 2014, pp. 233–245. https://doi.org/10.2514/1.B34692

[20] Ashida, Y., Yamakawa, H., Funaki, I., Usui, H., Kajimura, Y., and Kojima, H., "Thrust Evaluation of Small-Scale Magnetic Sail Spacecraft by Three-Dimensional Particle-in-Cell Simulation," *Journal of Propulsion and Power*, Vol. 30, No. 1, Jan. 2014, pp. 186–196.
https://doi.org/10.2514/1.B35026

[21] Funaki, I., and Yamakawa, H., "The Challenge of Magnetoplasma Sail Propulsion for Deep Space Explorations," *Journal of Plasma and Fusion Research*, Vol. 83, No. 3, 2007, pp. 281–284.

[22] Fujimoto, T., Otsu, H., Funaki, I., and Yamagiwa, Y., "MHD Analysis of Magnetic Diffusion Effect on Magneto Plasma Sail," *Transactions of The Japan Society for Aeronautical and Space Science*, Vol. 53, No. 180, 2010, pp. 84–90.
https://doi.org/10.2322/tjsass.53.84

[23] Funaki, I., Kojima, H., Yamakawa, H., Shimizu, Y., Toki, K., Nakayama, Y., Fujita, K., Ogawa, H., and Shinohara, S., "Development of an Experimental Simulator of Magnetic Sail," *Journal of The Japan Society for Aeronautical and Space Sciences*, Vol. 54, No. 634, 2006, pp. 501–509.
https://doi.org/10.2322/JJSASS.54.501

[24] Barmin, A. A., Kulikovskiy, A. G., and Pogorelovc, N. V., "Shock-Capturing Approach and Nonevolutionary Solutions in Magnetohydrodynamics," *Journal of Computational Physics*, Vol. 126, No. 1, June 1996, pp. 77–90.
https://doi.org/10.1006/jcph.1996.0121

[25] Powell, K. G., Roe, P. L., Linde, T. J., Gombosi, T. I., and De Zeeuw, D. L., "A Solution-Adaptive Upwind Scheme for Ideal Magnetohydrodynamics," *Journal of Computational Physics*, Vol. 154, No. 2, Sep. 1999, pp. 284–309.
https://doi.org/10.1006/jcph.1999.6299

[26] Brio, M., and Wu, C. C., "An Upwind Differencing Scheme for the Equations of Ideal Magnetohydrodynamics," *Journal of Computational Physic*s, Vol. 75, No. 2, Apr. 1988, pp. 400–422.
https://doi.org/10.1016/0021-9991(88)90120-9

[27] Ryu, D., and Jones, T. W., "Numerical Magnetohydrodynamics in Astrophysics: Algorithm and Tests for One-Dimensional Flow," *The Astrophysical Journal*, Vol. 442, No. 1, Mar. 1995, pp. 228–258.
https://doi.org/10.1086/175437